Polarized spectroscopy of Ho:$YAlO_3$ crystals for 2 μm and 3 μm lasers

Ghassen Zin Elabedine[a], Pavel Loiko[b], Simone Normani[b], Rosa Maria Solé[a], Alain Braud[b], Patrice Camy[b], Elena Dunina[c], Liudmila Fomicheva[d], Alexey Kornienko[c], Weidong Chen[e], Dunlu Sun[f], Peixiong Zhang[g], Xavier Mateos[a,#,*], Uwe Griebner[e], and Valentin Petrov[e]

[a]Universitat Rovira i Virgili, URV, Física i Cristal·lografia de Materials (FiCMA), Marcel·lí Domingo 1, 43007 Tarragona, Spain
[b]Centre de Recherche sur les Ions, les Matériaux et la Photonique (CIMAP), UMR 6252 CEA-CNRS-ENSICAEN, Université de Caen Normandie, 6 Boulevard Maréchal Juin, 14050 Caen, France
[c]Vitebsk State Technological University, 210035 Vitebsk, Belarus
[d]BIP - University of Law and Social-Information Technologies, Department of IT and Mathematics, 3 Korol St., 220004 Minsk, Belarus
[e]Max Born Institute for Nonlinear Optics and Short Pulse Spectroscopy, Max-Born-Str. 2a, 12489 Berlin, Germany
[f]Anhui Institute of Optics and Fine Mechanics, Hefei Institutes of Physical Science, Chinese Academy of Sciences, 230031 Hefei, China
[g]Department of Optoelectronic Engineering, Jinan University, 510632 Guangzhou, China
[#]Serra Húnter Fellow, Spain

ABSTRACT

We report on polarized spectroscopic properties of Ho^{3+} ions in orthorhombic (sp. gr. *Pnma*) yttrium orthoaluminate $YAlO_3$ crystals for laser development at 2 μm and 3 μm. This includes polarized Raman, absorption and luminescence spectra, fluorescence lifetime measurements and Stark energy-level study. The transition intensities for Ho^{3+} ions are calculated using the Judd-Ofelt theory. The peak stimulated-emission cross-sections are 2.01×10^{-20} cm^2 at 1977 nm ($^5I_7 \rightarrow {}^5I_8$) and 2.31×10^{-20} cm^2 at 2918 nm ($^5I_6 \rightarrow {}^5I_7$) for light polarization $\boldsymbol{E} \parallel \boldsymbol{b}$. For both transitions, pump-induced polarization-switching is expected. The fluorescence lifetimes of the $^5I_7$ and $^5I_6$ Ho^{3+} manifolds are 7.27 and 0.36 ms, respectively (for 1 at.% Ho^{3+}-doping).

Keywords: yttrium aluminate, holmium ions, laser crystal, optical spectroscopy, Judd-Ofelt analysis.

1. INTRODUCTION

The Holmium ion (Ho^{3+}), with an electronic configuration of $[Xe]4f^{10}$, plays a crucial role in solid-state laser technology due to its appealing emission properties. Its main emission, corresponding to a transition from the first excited-state ($^5I_7$) to the ground-state ($^5I_8$), is slightly above 2 μm, which is relatively eye-safe [1]. Another emission channel slightly below 3 μm is due to the $^5I_6 \rightarrow {}^5I_7$ transition, Fig. 1(a). 2-μm Ho-lasers find applications in remote sensing, wind mapping [2,3], and laser surgery, as their emission aligns with a local maximum of water absorption in bio-tissues and the atmosphere [4]. This wavelength range is also ideal for pumping mid-IR optical parametric oscillators (OPOs) and optical parametric amplifiers (OPAs) based on non-oxide nonlinear crystals [5]. Emission near 3 μm on the other side coincides with the absolute maximum of water absorption which corresponds to minimum penetration depth [4]. All emerging applications related to the development of continuous-wave (CW), Q-switched, and mode-locked (ML) bulk or thin-disk lasers operating in these wavelength ranges, require a thorough characterization of the applicable Ho-doped crystals.

*e-mail: xavier.mateos@urv.cat

Solid State Lasers XXXIII: Technology and Devices, edited by W. Andrew Clarkson, Ramesh K. Shori, Proc. of SPIE Vol. 12864, 128640V · © 2024 SPIE
0277-786X · doi: 10.1117/12.3002400

Yttrium aluminium perovskite ($YAlO_3$ or YAP) is a crystalline material with remarkable optical, thermal, and mechanical properties, which, similar to the well-known yttrium aluminium garnet ($Y_3Al_5O_{12}$ or YAG), is a compound in the Al_2O_3-Y_2O_3 system [6]. However, in contrast to the cubic YAG, YAP belongs to the orthorhombic symmetry class (space group D_{2h}^{16} - *Pnma*), which renders it biaxial and anisotropic in nature.

The intrinsic birefringence of $YAlO_3$ crystals and the related anisotropy of the Ho^{3+} emission in this host determine the linearly polarized emission from such solid-state lasers [6,7]. This is especially valuable for applications in nonlinear optical, THz and Raman frequency conversion, where linearly polarized laser sources are needed. It also suppresses thermally induced birefringence effects typical for cubic crystals such as YAG. Additionally, $YAlO_3$ has a relatively low phonon energy compared to other oxide laser hosts (551 cm^{-1}), see Fig. 1(b), due to the absence of tetrahedral molecular groups in its lattice. The low phonon energies diminish the rates of multiphonon non-radiative relaxation, which is particularly relevant for the development of lasers emitting in the wavelength range between 2 and 3 μm, with the latter considered to be a rough upper limit for any oxide based solid-state laser [8]. The $^5I_6 \rightarrow {}^5I_7$ Ho^{3+} laser transition in $YAlO_3$ was known from Xe flash lamp pumping [9] but resonant laser pumping with a tuning element resulted in emission up to 3.017 μm [10].

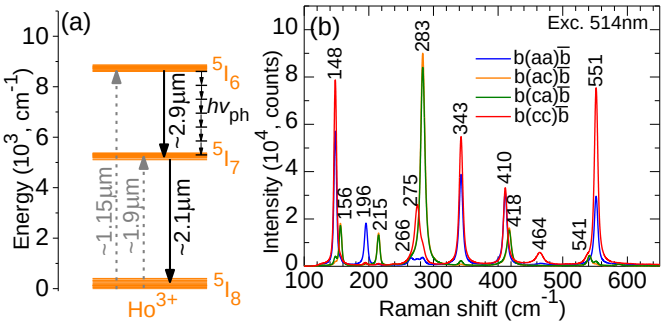

Figure 1. (a) A simplified energy-level diagram of the Ho^{3+} ion showing pump and laser transitions, $h\nu_{ph}$ – phonon energy; (b) polarized Raman spectra of undoped $YAlO_3$ for the $\boldsymbol{b}(ij)\bar{\boldsymbol{b}}$ geometry (i, j = $\boldsymbol{a}$, $\boldsymbol{c}$); Porto's notations are used, and the excitation wavelength is λ_{exc} = 514 nm.

Reliable spectroscopic data are instrumental to optimize the design of Ho:$YAlO_3$ lasers. In the present work, we report on a comprehensive spectroscopic study of Ho:$YAlO_3$ crystals bearing in mind their potential for laser development around 2 and 3 μm. In particular, we focus on the polarization anisotropy of the Ho^{3+} emission properties in this optically biaxial material which can explain the polarization switching behavior often observed in Ho:$YAlO_3$ lasers.

2. RESULTS AND DISCUSSION

2.1 Optical absorption

The optical indicatrix frame for $YAlO_3$ coincides with the crystallographic axes. With the convention $n_x < n_y < n_z$ for the principal refractive indices the correspondence is $xyz \equiv bac$. We adopt here the *Pnma* space group for $YAlO_3$ (if the *Pbnm* space group is used instead, the correspondence would be $xyz \equiv cba$ [6]). In this work, we denote the principal light polarizations as $\boldsymbol{E} \parallel \boldsymbol{a}, \boldsymbol{b}, \boldsymbol{c}$. A cube from Ho:$YAlO_3$ was well oriented in this frame and all six faces were polished. Using a single sample rules out any dependence of the results on quality or doping concentration variation. The absorption spectrum in the range of 350 – 2150 nm was acquired using a spectrophotometer (Lambda 1050, Perkin Elmer, spectral resolution: 0.3 – 1 nm) and a Glan-Taylor polarizer.

The polarized absorption spectrum of Ho:$YAlO_3$ is shown in Fig. 2. It is expressed in absorption cross-sections ($\sigma_{abs} = \alpha_{abs}/N_{Ho}$, α_{abs} – absorption coefficient). The ion density for the 1 at.% Ho^{3+}-doped $YAlO_3$ crystal was 1.97×10^{20} at/cm^3. Ho^{3+} has an electronic configuration of [Xe]$4f^{10}$ with a ground-state $^5I_8$. In the absorption spectrum, the bands are assigned to electronic transitions from the $^5I_8$ Ho^{3+} manifold to the excited states from $^5I_7$ to $^5G_4$. The absorption spectra are strongly polarized. They are structured suggesting an insignificant temperature broadening for this material owing to a weak electron-phonon interaction.

The $^5I_8 \rightarrow {}^5I_7$ transition around 1.9 µm is used for resonant (in-band) pumping of Ho lasers operating at ~2 µm [4]. It can be addressed by Tm-fiber lasers or GaSb-based laser diodes. For this transition, the maximum σ_{abs} is 1.29×10^{-20} cm^2 at 1977 nm, corresponding to an absorption bandwidth (full width at half maximum, FWHM) of 7 nm, for light polarization $\boldsymbol{E} \parallel \boldsymbol{b}$. For the other two polarizations, the absorption is weaker, and the dominant absorption peak appears at a shorter wavelength of 1929 nm, $\sigma_{abs} = 0.98\times10^{-20}$ cm^2 ($\boldsymbol{E} \parallel \boldsymbol{a}$) and $\sigma_{abs} = 1.18\times10^{-20}$ cm^2 ($\boldsymbol{E} \parallel \boldsymbol{c}$). The absorption bandwidth is similar, 6 and 7 nm, respectively.

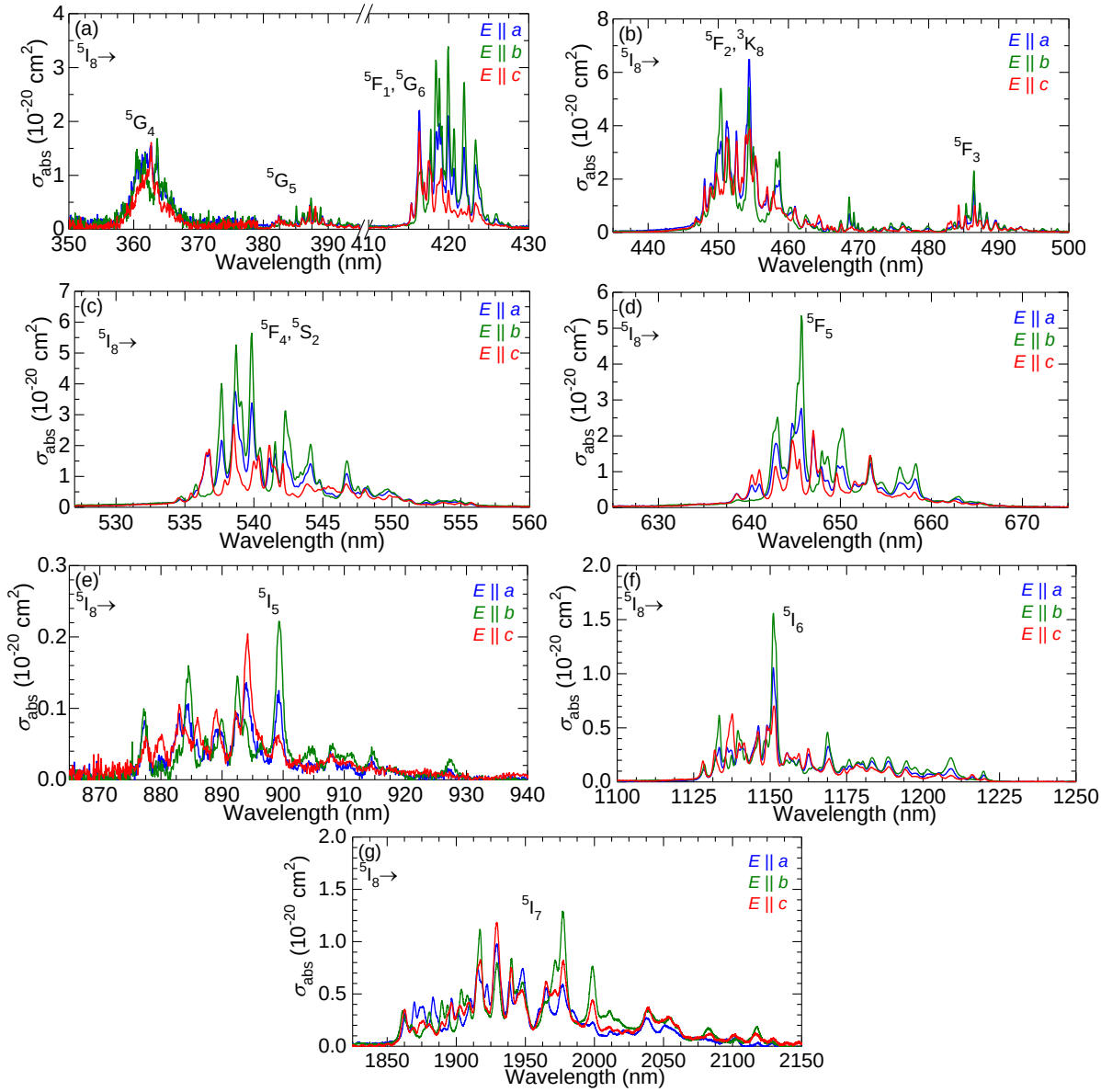

Figure 2. (a)-(f) Polarized absorption spectrum of Ho^{3+}:$YAlO_3$, light polarizations: $\boldsymbol{E} \parallel \boldsymbol{a}$, $\boldsymbol{b}$, $\boldsymbol{c}$ (space group *Pnma*).

The $^5I_8 \rightarrow {}^5I_6$ transition around 1.15 µm is relevant for resonant pumping of Ho lasers emitting at ~2.9 µm. It matches the emission of Raman fiber lasers [11]. In this spectral range, the maximum σ_{abs} amounts to 1.56×10^{-20} cm^2 at 1151 nm (for light polarization $\boldsymbol{E} \parallel \boldsymbol{b}$) with a FWHM of 2 nm. At the same peak wavelength, the absorption cross-sections for the other two polarizations are lower, $\sigma_{abs} = 1.06\times10^{-20}$ cm^2 ($\boldsymbol{E} \parallel \boldsymbol{a}$) and $\sigma_{abs} = 0.70\times10^{-20}$ cm^2 ($\boldsymbol{E} \parallel \boldsymbol{c}$).

2.2 Judd-Ofelt analysis

The transition intensities of Ho^{3+} ions in the $YAlO_3$ crystal were calculated using the Judd-Ofelt (J-O) formalism by applying both the standard J-O theory [12,13], and its modification accounting for intermediate configuration interaction with the excited configuration of the opposite parity $4f^{n-1}5d^1$ (ICI) [14,15]. The set of squared reduced matrix elements $U^{(k)}$ (k = 2, 4, 6) was calculated using the free-ion parameters reported by Tanner *et al.* [16]. The contribution of magnetic dipole (MD) transitions, following the selection rules $\Delta S = 0$, $\Delta L = 0$, $\Delta J = 0, \pm 1$, was computed within the Russell-Saunders approximation based on the wave functions of the Ho^{3+} free ion.

The experimental absorption oscillator strengths $\langle f_{exp} \rangle$ are listed in Table 1. Here, the polarization averaging is performed as $\langle .. \rangle = 1/3(\boldsymbol{a} + \boldsymbol{b} + \boldsymbol{c})$. The absorption oscillator strengths calculated using both the J-O and ICI models, f^{Σ}_{calc}, are also included in Table 1, where the superscript "Σ" indicates the total (ED + MD, ED - electric dipole) value. The intensity parameters are as follows: $\Omega_2 = 1.280$, $\Omega_4 = 3.708$, $\Omega_6 = 2.066$ [10^{-20} cm^2] (the standard J-O theory) and $\Omega_2 = 1.328$, $\Omega_4 = 3.074$, $\Omega_6 = 4.424$ [10^{-20} cm^2] and $R_2 = 0.026$, $R_4 = -0.031$ and $R_6 = 0.074$ [10^{-4} cm] (the ICI model). Here, the R_k (k = 2, 4, 6) parameters describe the configuration interaction.

The root-mean-square (r.m.s.) deviation between the experimental and calculated absorption oscillator strengths is notably reduced when employing the ICI model (0.209), compared to the standard J-O theory (0.362). In addition, the application of the standard model underestimates the radiative lifetime of the lower excited state ($^5I_7$). Consequently, the ICI model was adopted for subsequent calculations.

Table 1. Experimental and calculated absorption oscillator strengths for the 1 at.% Ho:$YAlO_3$ crystal. E_J – energy range; $\langle \Gamma \rangle = \int \langle \sigma_{abs}(\lambda) \rangle d\lambda$ – integrated absorption cross-section; $\langle f_{exp} \rangle$, f^{Σ}_{calc} – experimental and calculated absorption oscillator strengths, respectively; <..> indicates polarization averaging; ED, MD – electric dipole and magnetic dipole contributions, respectively.

Transition $^5I_8 \rightarrow {}^{2S+1}L_J$	E_J, cm^{-1}	$\langle \Gamma \rangle \times 10^{20}$, $cm^2 nm$	$\langle f_{exp} \rangle$, 10^{-6}	f^{Σ}_{calc}, 10^6 J-O	f^{Σ}_{calc}, 10^6 ICI
$^5I_7$	4894 - 5340	73.082	2.155	$2.271^{ED}+0.579^{MD}$	$1.637^{ED}+0.579^{MD}$
$^5I_6$	8313 - 8786	16.858	1.412	1.612^{ED}	1.281^{ED}
$^5I_5$	11004 - 11398	1.812	0.256	0.308^{ED}	0.271^{ED}
$^5F_5$	15214 - 15615	19.491	5.231	5.112^{ED}	5.128^{ED}
$^5F_4 + {}^5S_2$	18242 - 18610	17.297	6.655	6.388^{ED}	6.762^{ED}
$^5F_3 + {}^5F_2 + {}^3K_8 + {}^5G_6$	20422 - 22265	31.076	16.789	$16.707^{ED}+0.123^{MD}$	$16.675^{ED}+0.123^{MD}$
$^5G_5$	23614 - 24018	8.417	5.401	5.606^{ED}	5.451^{ED}
$^3K_7 + {}^5G_4$	25625 - 26127	1.848	1.379	$0.891^{ED}+0.005^{MD}$	$1.016^{ED}+0.005^{MD}$
$^5G2_5 + {}^3H_6$	27377 - 27868	7.138	6.135	5.966^{ED}	6.106^{ED}
r.m.s. deviation				*0.362*	*0.209*

The probabilities of spontaneous radiative transitions $A^{\Sigma}_{calc}(JJ')$, the luminescence branching ratios $\beta(JJ')$, and the radiative lifetimes of the excited states τ_{rad} are compiled in Table 2, as determined using the ICI approximation. Here, we considered only the transitions from the $^5I_7$ and $^5I_6$ upper laser levels. Their radiative lifetimes are 6.19 ms and 2.77 ms, respectively, and the luminescence branching ratio for the $^5I_6 \rightarrow {}^5I_7$ transition around 2.9 μm is as high as 16.3%.

Table 2. Calculated probabilities of emission transitions from the $^5I_7$ and $^5I_6$ manifolds of Ho^{3+} ions in the $YAlO_3$ crystal: $\langle \lambda_{em} \rangle$ - mean emission wavelength, A^{Σ}_{calc} – probability of spontaneous radiative transitions (ED + MD), $\beta(JJ')$ – luminescence branching ratio, A_{tot} and τ_{rad} – total probability of radiative spontaneous transitions and radiative lifetime of the excited state, respectively.

J→	**J'**	$\langle \lambda_{em} \rangle$, **nm**	$A^{\Sigma}_{calc}(JJ')$, s^{-1}	$\beta(JJ')$	A_{tot}, s^{-1}	τ_{rad}, **ms**
$^5I_7$	$^5I_8$	1947.0	$119.2^{ED} + 42.40^{MD}$	1	161.6	6.19
$^5I_6$	$^5I_7$	2892.7	$37.15^{ED} + 21.57^{MD}$	0.163	360.41	2.77
$^5I_6$	$^5I_8$	1163.7	301.7^{ED}	0.837		

Weber *et al.* reported on the transition intensities for Ho:$YAlO_3$ based on unpolarized absorption spectra [17]. Their analysis employing the standard J-O formalism yielded $\tau_{rad}(^5I_7)$ = 6.41 ms, $\tau_{rad}(^5I_6)$ = 3.00 ms and $\beta(^5I_6 \rightarrow {}^5I_7)$ = 15.6% which agrees with our refined data.

2.3 Stimulated-emission cross-sections

The luminescence spectra were acquired using an optical spectrum analyzer (Yokogawa AQ6376) purged with N_2 gas to reduce the impact of structured water vapor absorption which spectrally overlaps with both Ho^{3+} ion emissions that we study. A large mode area zirconium fluoride (ZrF_4) fiber was employed for collecting the luminescence. A metal-grid polarizer was used for recording polarized spectra. For excitation, a Ti:Sapphire laser tuned to ~900 nm was employed.

The stimulated-emission (SE) cross-sections, σ_{SE}, were calculated employing the Füchtbauer–Ladenburg (F-L) formula [18]:

$$\sigma_{SE}^{i}(\lambda) = \frac{\lambda^5}{8\pi\langle n\rangle^2 \tau_{rad} c} \frac{\beta(JJ')W_i(\lambda)}{1/3\sum_{j=a,b,c}\int \lambda W_j(\lambda)d\lambda}, \quad (1)$$

where, λ denotes the wavelength of light, $\langle n\rangle$ is the mean refractive index at the average emission wavelength, c is the speed of light, τ_{rad} stands for the radiative lifetime of the emitting state ($^5I_6$ or $^5I_7$), $W_i(\lambda)$ signifies the luminescence spectrum calibrated for the spectral response of the setup, and i = ***a***, ***b***, ***c*** indicates the light polarization.

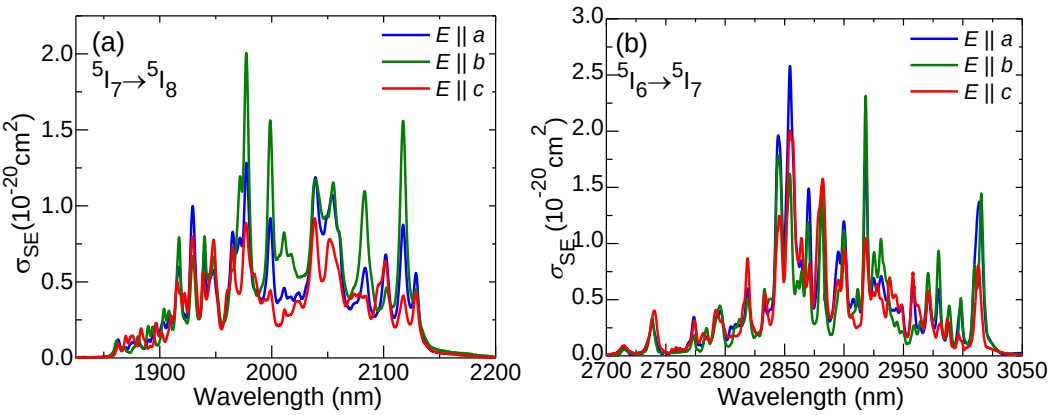

Figure 3. Stimulated-emission (SE) cross-sections, σ_{SE}, of Ho^{3+} in $YAlO_3$: (a) the $^5I_7 \rightarrow {}^5I_8$ transition; (b) the $^5I_6 \rightarrow {}^5I_7$ transition. Light polarizations: ***E*** || ***a***, ***b***, ***c***.

The polarized σ_{SE} spectra for Ho^{3+}:$YAlO_3$ are depicted in Fig. 3. For the quasi-three-level $^5I_7 \rightarrow {}^5I_8$ transition giving rise to 2 μm lasing, in the spectral range where laser emission is expected, the maximum SE cross-section is observed for light polarization ***E*** || ***b***, with a value of 2.01×10^{-20} cm^2 at 1977 nm. Ho^{3+} ions exhibit strong polarization anisotropy of their emission properties as for the other two polarizations the SE cross-sections are lower, $\sigma_{SE} = 1.28\times10^{-20}$ cm^2 at 1977 nm (***E*** || ***a***) and $\sigma_{SE} = 0.92\times10^{-20}$ cm^2 at 2038 nm (***E*** || ***c***). This suggests natural selection of linearly polarized emission from Ho:$YAlO_3$ lasers, along the ***b***- or ***a***-axis, depending on the chosen cut.

For the $^5I_6 \rightarrow {}^5I_7$ transition responsible for laser emission near 2.9 μm, the maximum σ_{SE} is determined to be 2.58×10^{-20} cm^2 at 2854 nm for ***E*** || ***a*** light polarization. Due to the long luminescence lifetime of the terminal level for this transition and the occurrence of resonant excited-state absorption on the same transition, $^5I_7 \rightarrow {}^5I_6$, 2.9-μm Ho-lasers typically operate at longer wavelengths than their zero-phonon lines. The corresponding peak σ_{SE} values are $\sigma_{SE} = 2.58\times10^{-20}$ cm^2 at 2854 nm (***E*** || ***a***), $\sigma_{SE} = 2.31\times10^{-20}$ cm^2 at 2918 nm (***E*** || ***b***) and $\sigma_{SE} = 2.00\times10^{-20}$ cm^2 at 2855 nm (***E*** || ***c***).

2.4 Luminescence decay

The luminescence dynamics study involved a nanosecond optical parametric oscillator (Horizon, Continuum), a 1/4 m monochromator (Oriel 77200), a fast InGaAs detector, and an 8 GHz digital oscilloscope (DSA70804B, Tektronix). The decay from the $^5I_7$ and $^5I_6$ states of Ho^{3+} ions was studied under resonant excitation: λ_{exc} = 1930 nm and 895 nm, and

detected at 2020 nm and 1204 nm, respectively. The studied crystal, 1 at.% Ho:$YAlO_3$, was finely ground into a powder to reduce the effect of radiation trapping (reabsorption) on the measured lifetimes.

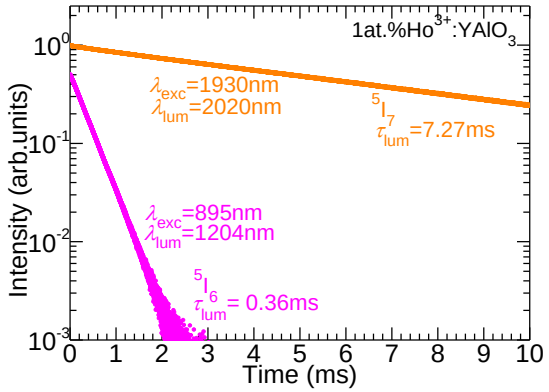

Figure 4. Luminescence decay curves from the $^5I_6$ and $^5I_7$ Ho^{3+} states measured under resonant excitation for a 1 at.% Ho:$YAlO_3$ crystal (a finely powdered sample), λ_{exc} and λ_{lum} – excitation and luminescence wavelengths, respectively, τ_{lum} – luminescence lifetime.

The measured luminescence decay curves, plotted on a semi-logarithmic scale, are presented in Fig. 4. The luminescence decay times τ_{lum} are 7.27 ms for the $^5I_7$ state and 0.36 ms for the $^5I_6$ state. The τ_{lum} value for the $^5I_7$ manifold is longer than the radiative lifetime calculated using the ICI model (6.19 ms) most probably due to the residual reabsorption. Šulc *et al.* reported a $^5I_7$ luminescence lifetime of τ_{lum} = 7.1 ms for a 0.34 at.% Ho^{3+}-doped $YAlO_3$, in line with our result [19]. The luminescence lifetime for the $^5I_6$ manifold is much shorter than the calculated radiative lifetime (2.77 ms) due to a notable multiphonon non-radiative relaxation from this level: the energy-gap to the lower-lying state is 3310 cm^{-1}, and the maximum phonon energy of the $YAlO_3$ host crystal is 551 cm^{-1}, so that a 6-phonon process is expected.

2.5 Crystal-field splitting

To resolve the Stark splitting of the $^5I_8$ to $^5I_6$ Ho^{3+} multiplets in $YAlO_3$, polarized absorption and luminescence spectra were measured at 12 K where virtually all the ions rest in the lowest-energy Stark sub-level of a given manifold, as illustrated in Figure 5. The low-temperature (LT) absorption spectra were plotted versus the photon energy and the LT emission spectra - versus E_{ZPL} – photon energy (both expressed in cm^{-1}) revealing the splitting of the excited-states ($^5I_7$, $^5I_6$) and the ground-state ($^5I_8$), respectively. An APD DE-202 closed-cycle cryo-cooler equipped with an APD HC 2 Helium vacuum cryo-compressor and a Laceshore 330 temperature controller were used for the LT studies.

Table 3. Experimental crystal-field splitting of the three lowest Ho^{3+} multiplets in the $YAlO_3$ crystal.

$^{2S+1}L_J$	Energy E, cm^{-1}	Number		ΔE, cm^{-1}
		Theor.	Exp.	
$^5I_8$	0, 21, 52, 68, 85, 141, 156, 164, 169, 203, 234, 272, 335, 370, 386, 421, 446	17	17	446
$^5I_7$	5141, 5180, 5185, 5217, 5221, 5228, 5268, 5287, 5311, 5319, 5335, 5350, 5355, 5368, 5373	15	15	232
$^5I_6$	8683, 8688, 8728, 8734, 8758, 8763, 8770, 8778, 8793, 8834, 8838, 8865, 8869	13	13	186

In $YAlO_3$, the dopant Ho^{3+} ions replace for the Y^{3+} host-forming cations in a single type of sites of C_s symmetry with a distorted XII-fold oxygen coordination. For C_s symmetry sites, each $^{2S+1}L_J$ multiplet with an integer J is split into a total of $2J + 1$ sub-levels (17 for $^5I_8$, 15 for $^5I_7$ and 13 for $^5I_6$). All Stark sub-levels were successfully identified. The assignment of the LT spectra followed the early work of Antonov *et al.* [20] considering that the authors performed their studies at 77 K where a noticeable thermal population of the lower-lying Stark sub-levels takes place, so that not all the Stark sub-levels were previously resolved. The experimental energies of the Stark sub-levels of the $^5I_8$ to $^5I_6$ Ho^{3+} multiplets are listed in Table 3. The total Stark splitting ΔE of the $^5I_8$ and $^5I_7$ terminal laser levels is relatively large: 446 cm^{-1} and 232 cm^{-1}, respectively, and is thus responsible for the relatively broadband emission of Ho^{3+} in $YAlO_3$.

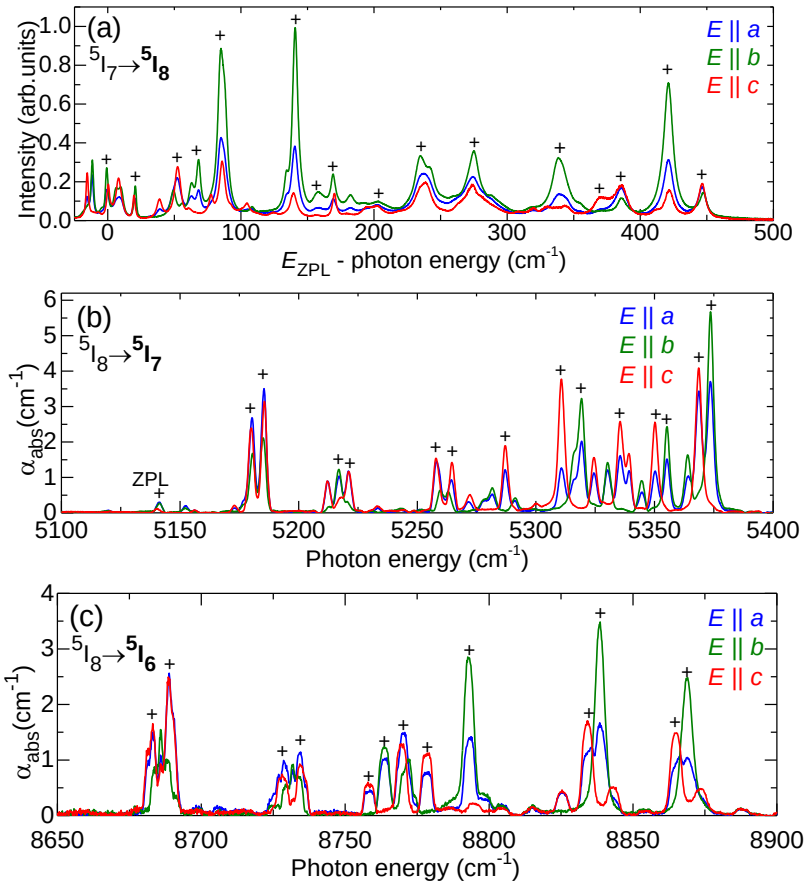

Figure 5. Low-temperature (12 K) spectroscopy of Ho^{3+} ions in $YAlO_3$: (a) LT luminescence spectra, the $^5I_7 \rightarrow {}^5I_8$ transition; (b),(c) LT absorption spectra: (b) the $^5I_8 \rightarrow {}^5I_7$ transition; (c) the $^5I_8 \rightarrow {}^5I_6$ transition; "+" indicates peaks assigned to electronic transitions of Ho^{3+} ions in C_s sites.

3. CONCLUSIONS

To conclude, orthorhombic $YAlO_3$ crystals doped with Ho^{3+} ions exhibit attractive spectroscopic properties for the development of 2 μm and 3 μm lasers, namely (i) relatively broad and intense emission bands due to the $^5I_7 \rightarrow {}^5I_8$ and $^5I_6 \rightarrow {}^5I_7$ transitions for polarized light, (ii) large Stark splitting of the terminal laser manifolds ($^5I_8$ and $^5I_7$), and (iii) a relatively long $^5I_7$ luminescence lifetime and a reasonably long lifetime of the $^5I_6$ manifold (considering a notable non-radiative path from this state in oxides). Coupled with the good thermal and thermo-mechanical properties of $YAlO_3$ as a host matrix and its moderately high phonon energy, Ho:$YAlO_3$ is of great interest for power-scalable operation around 2 μm both in bulk and thin-disk laser geometries. The long luminescence lifetime of the $^5I_7$ state (~7 ms) and the large Stark splitting of the ground-state (446 cm^{-1}) support low-threshold laser operation, while the anisotropy of the laser gain underlines linearly polarized emission. However, also two deficiencies can be predicted: (i) due to the close SE cross-sections spectra for orthogonal eigen-polarization states and expected anisotropy of thermal lensing properties, Ho:$YAlO_3$ may be prone to polarization switching upon changing the pump level, output coupling or while tuning the wavelength; (ii) the suggested weak electron-phonon coupling in this matrix results in structured emission spectra with narrow individual emission peaks possibly limiting the generation of ultrashort (femtosecond) pulses from mode-locked lasers; it is difficult to predict the natural selection of the polarization from the present results in the case of broadband oscillation as in mode-locked lasers. The latter can be overcome by employing compositionally "mixed" (solid-solution) Ho:(Y,Gd,Lu)AlO_3 crystals or by combining two of the principal polarizations into an eigen-polarization in a special polarization-selective geometry of the active element.

ACKNOWLEDGEMENTS

Grant PID2022-141499OB-I00 funded by MCIN/AEI/ 10.13039/501100011033; Grant PECT “Cuidem el que ens uneix", operation 4 Sensòrica; Act 4 Fotònica” PR15-020174 co-financed by the European Regional Development Fund “ERDF A way of making Europe” through the ERDF Catalonia Operational Programme 2014-2020; French Agence Nationale de la Recherche (ANR) (LabEx EMC3 (ANR-10-LABX-09-01); SPLENDID2 (ANR-19-CE08-0028)); Normandy Region (“RELANCE” Chair of Excellence project).

REFERENCES

[1] Walsh, B. M., Barnes, N. P. and Di Bartolo, B., “Branching ratios, cross sections, and radiative lifetimes of rare earth ions in solids: Application to Tm^{3+} and Ho^{3+} ions in $LiYF_4$,” J. Appl. Phys. **83**(5), 2772–2787 (1998).

[2] Taczak, T. M. and Killinger, D. K., “Development of a tunable, narrow-linewidth, cw 2.066-μm Ho:YLF laser for remote sensing of atmospheric CO_2 and H_2O,” Appl. Opt. **37**(36), 8460–8476 (1998).

[3] Singh, U. N., Walsh, B. M., Yu, J., Petros, M., Kavaya, M. J., Refaat, T. F. and Barnes, N. P., “Twenty years of Tm:Ho:YLF and LuLiF laser development for global wind and carbon dioxide active remote sensing,” Opt. Mater. Express **5**(4), 827–837 (2015).

[4] Scholle, K., Lamrini, S., Koopmann, P. and Fuhrberg, P., “2 μm laser sources and their possible applications”, Ch. 21 of *Frontiers in Guided Wave Optics and Optoelectronics*, ed. by Pal, B. Intech (2010), pp. 471- 500.

[5] Petrov, V., “Frequency down-conversion of solid-state laser sources to the mid-infrared spectral range using non-oxide nonlinear crystals,” Prog. Quantum Electron. **42**, 1–106 (2015).

[6] Weber, M. J., Bass, M., Andringa, K., Monchamp, R. R. and Comperchio, E., “Czochralski growth and properties of $YAlO_3$ laser crystals,” Appl. Phys. Lett. **15**(10), 342–345 (1969).

[7] Weber, M. J., Bass, M., Varitimos, T. E. and Bua, D. P., "Laser action from Ho^{3+}, Er^{3+}, and Tm^{3+} in $YAlO_3$," IEEE J.Quantum Electron. **9**(11), 1079–1086 (1973).

[8] Kaminskii, A. A., “Laser crystals and ceramics: recent advances,” Laser & Photon. Rev. **1**, 93–177 (2007).

[9] Kaminskii, A. A., Butaeva, T. I., Ivanov, A. O., Mochalov, I. V., Petrosian, A. G., Rogov, G. I. and Fedorov, V. A., "New data on stimulated emission of crystals containing Er^{3+} and Ho^{3+} ions," Sov. Tech. Phys. Lett. **2**(9), 308–310 (1976) [transl. from Pis'ma v Zhurnal Tekhnicheskoi Fiziki **2**(9), 787–793 (1976)].

[10] Bowman, S. R., Rabinovich, W. S. and Feldman, B.J., "Tuning the 3 μm Ho:$YAlO_3$ laser," Advanced Solid-State Lasers 1990, OSA Proc. Ser. Vol. 6 (1990), pp. 254–256.

[11] Qiao, Y., Sun, D., Zhang, H., Luo, J., Quan, C., Hu, L., Han, Z., Dong, K., Chen, Y. and Cheng, M., “Spectroscopy and 3.01 μm laser performance of Ho:YAP oxide crystal pumped by 1150 nm Raman laser,” Opt. Laser Technol. **157**, 108728 (2023).

[12] Judd, B. R., “Optical absorption intensities of rare-earth ions,” Phys. Rev. **127**(3), 750 (1962).

[13] Ofelt, G. S., “Intensities of crystal spectra of rare-earth ions,” J. Chem. Phys. **37**(3), 511–520 (1962).

[14] Loiko, P., Volokitina, A., Mateos, X., Dunina, E., Kornienko, A., Vilejshikova, E., Aguiló, M. and Díaz, F., “Spectroscopy of Tb^{3+} ions in monoclinic $KLu(WO_4)_2$ crystal application of an intermediate configuration interaction theory,” Opt. Mater. **78**, 495–501 (2018).

[15] Kornienko, A. A., Kaminskii, A. A. and Dunina, E. B., “Dependence of the line strength of f–f transitions on the manifold energy. II. Analysis of Pr^{3+} in $KPrP_4O_{12}$,” Phys. Status Solidi (b) **157**(1), 267–273 (1990).

[16] Tanner, P. A., Kumar, V. R. K., Jayasankar, C. K. and Reid, M. F., "Analysis of spectral data and comparative energy level parametrizations for Ln^{3+} in cubic elpasolite crystals," J. Alloys Compd. **215**(1-2), 349-370 (1994).

[17] Weber, M. J., Matsinger, B. H., Donlan, V. L. and Surratt, G. T., "Optical transition probabilities for trivalent holmium in LaF_3 and $YAlO_3$," J. Chem. Phys. **57**(1), 562-567 (1972).

[18] Aull, B. F. and Jenssen, H. P., “Vibronic interactions in Nd:YAG resulting in nonreciprocity of absorption and stimulated emission cross sections,” IEEE J. Quantum Electron. **18**(5), 925–930 (1982).

[19] Šulc, J., Němec, M., Vyhlídal, D., Jelínková, H., Nejezchleb, K. and Polák, J., “Holmium doping concentration influence on Ho:YAG crystal spectroscopic properties,” Proc. SPIE **11664**, 105–115 (2021).

[20] Antonov, V. A., Arsenev, P. A., Bienert, K. E. and Potemkin, A. V., “Spectral properties of rare-earth ions in $YAlO_3$ crystals,” Phys. Status Solidi (a) **19**(1), 289–299 (1973).